Available online at www.sciencedirect.com
ScienceDirect
Journal of Molecular Catalysis A: Chemical 279 (2008) 187–199
JOURNAL OF MOLECULAR CATALYSIS A: CHEMICAL
www.elsevier.com/locate/molcata

Palladium catalysts immobilized in thin films of ionic liquid for the direct addition of aniline to styrene

Carsten Sievers [a,1], Oriol Jiménez [a], Richard Knapp [a], Xilei Lin [b], Thomas E. Müller [a,*], Andreas Türler [b], Birgit Wierczinski [b], Johannes A. Lercher [a]

[a] *Department Chemie, Lehrstuhl II für Technische Chemie, Technische Universität München, Lichtenbergstr. 4, D-85747 Garching, Germany*
[b] *Department Chemie, Lehrstuhl für Radiochemie, Technische Universität München, Walther-Meissner-Str. 3, D-85748 Garching, Germany*

Available online 22 June 2007

Abstract

Immobilization of organometallic complexes in thin supported films of ionic liquid has been used to generate a new class of hydroamination catalysts. High activities for the addition of aniline to styrene were obtained with a bi-functional system comprising [Pd(DPPF)](CF$_3$CO$_2$)$_2$ and CF$_3$SO$_3$H immobilized in silica supported imidazolium salts. In this environment, the metal complexes are concluded to be enclosed in solvent cages of ion pairs of the ionic liquid. With increasing temperature, the imidazolium cations gain mobility until the solvent cages break down at a specific temperature, which is noticeable as phase transition. At temperatures below the phase transition, the catalytic activity was strongly influenced by the choice of the ionic liquid. At temperatures above the phase transition, the activity for formation of the Markownikoff product was, in contrast, nearly identical with all ionic liquids tested. Under these conditions, also the formation of the *anti*-Markownikoff product was observed.

Keywords: Hydroamination; Styrene; Aniline; Ionic liquid; Imidazolium; Supported catalyst; Immobilization; Palladium; Catalysis; Solvent effects; Polarity; MAS NMR

1. Introduction

Hydroamination offers a highly attractive pathway for the synthesis of nitrogen containing molecules, as new CN bonds are formed in a single reaction step from easily accessible alkenes and alkynes [1–3]. A number of homogeneous catalysts, such as titanium [4–6], rhodium [6,7], palladium [6,8] and ruthenium complexes [6,9], are known for the hydroamination of alkynes and dienes with anilines. Rhodium catalysts were reported for the addition of morpholine to styrene with *anti*-Markownikoff regioselectivity [10]. In a domino reaction, the rhodium-catalyzed amination of styrenes with anilines gives direct access to substituted quinolines [11]. As parallel reaction, the *anti*-Markownikoff hydroamination of styrene was also observed. Palladium catalysts can also be used in the hydroamination of vinyl-arenes with anilines and provide the Markownikoff product [12]. Electron rich anilines react more readily. It was noted that the presence of a Brønsted acid accelerates the reaction. Later, this was explained by more facile protolysis of the metal–carbon bond in the 2-ammonia-alkyl intermediate (rate determining step, r.d.s., *vide infra*) [13]. Unexpectedly high catalytic activities were also observed for molecular catalysts in two-phase systems, where the catalyst was dissolved in an ionic liquid (IL) [14,15]. This was explained by the polar environment, which stabilizes a polar transition state associated with the r.d.s.:

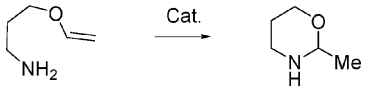

(1)

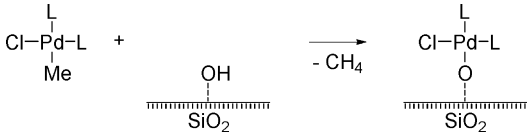

(2)

* Corresponding author. Tel.: +49 89 289 12827; fax: +49 89 289 13544.
E-mail address: thomas.mueller@tum.de (T.E. Müller).
[1] Present address: Georgia Institute of Technology, School of Chemical and Biomolecular Engineering, 311 Ferst Drive NW, Atlanta, GA 30332-0100, USA.

1381-1169/$ – see front matter © 2007 Elsevier B.V. All rights reserved.
doi:10.1016/j.molcata.2007.06.016

Table 1
Catalytic activity of supported palladium catalysts in the cyclization of 3-aminopropyl-vinylether [20]

Ligand[a]	Support	Pd loading (wt.%)	ToF (h^{-1})
DPPF	SiO_2	0.11	22.6
2-MePip	SiO_2	0.16	5.0
2-MePip	TiO_2	0.22	3.5
2-MePip	Al_2O_3	0.25	1.8

Reaction conditions: s/c = 200, diene/amine = 2, toluene, 70 °C.
[a] Immobilized catalysts were prepared by reaction of [PdClMe(PP)] with PP = 2-methylpiperidine (2-MePip) or 1,1′-bis(diphenylphosphino)ferrocene (DPPF) with hydroxyl groups on the surface of the support.

Although various homogeneous catalysts are known for hydroamination reactions, only few examples of heterogeneous catalysts have been reported [16]. The BASF process for *tert*-butylamine production from isobutene and ammonia takes place with more than 90% selectivity over a modified H-Beta zeolite [17,18]. Brønsted acidic zeolites also catalyze the addition of aryl-amines to 1,3-cyclohexadiene [19].

Recently, the cyclization of 3-aminopropyl-vinylether (Eq. (1)) was reported using palladium complexes supported on SiO_2, Al_2O_3, and TiO_2 [20]. Detailed characterization of the catalysts revealed the formation of a Pd–O bond between the palladium complex and the surface hydroxyl groups of the support (Eq. (2)). The activity decreased with the acidity of the support in the sequence $SiO_2 > TiO_2 > Al_2O_3$ (Table 1). This can be explained by decreasing Lewis acidity of the immobilized palladium.

High activities for inter- and intramolecular hydroamination of alkynes were observed, when catalytically active metal cations (such as Rh^+, Pd^{2+}, Cu^+, Zn^{2+}) were incorporated in zeolite H-Beta [21,22]. This was accounted to the simultaneous presence of Brønsted acidic hydroxyl groups and Lewis acidic metal cations. Apparently, particularly high activity in hydroamination is achieved with bi-functional catalysts.

Thus, it seemed highly promising to combine a Lewis acidic metal cation with a Brønsted acid to a bi-functional catalyst [23]. Anchoring of both catalytic functions in an ionic liquid [24,25] appeared appropriate for such an approach. The immobilization of organometallic complexes in thin films of ionic liquid has been previously explored successfully for other reactions [26,27], including Friedel–Crafts acylation of aromatic molecules [28,29] and hydroformylation [30]. The present work reports on immobilization of the two functions in a supported film of imidazolium salts and the preparation of well-tailored catalysts for the intermolecular hydroamination of styrene with aniline. Detailed characterization of the materials (see also [31]) and catalytic data (see also [32]) are related with each other for the first time.

2. Experimental

2.1. General

The ionic liquids 1-alkyl-3-methyl-imidazolium trifluoromethane sulphonate, alkyl = ethyl (EMIm), butyl (BMIm), hexyl (HMIm) and 1-hexyl-2,3-dimethyl-1-*H*-imidazolium trifluoromethane sulphonate (HM_2Im) with a maximum water and halide content of 32 and 322 ppm, respectively, were obtained from Merck. Palladium(II) trifluoroacetate, 1,1′-bis(diphenylphosphino)ferrocene (DPPF) (97%), trifluoromethane sulphonic acid (TfOH) (98%), dichloromethane (>99.5%), undecane (+99%), and aniline (99.5%) were obtained from Aldrich. Octane (>99%) and styrene (99.5%) were purchased from Fluka. The silica support Aerosil 355 was kindly provided by Degussa AG. All chemicals were used as received.

2.2. Preparation of the supported catalysts

$[Pd(CF_3CO_2)_2]$ and DPPF were suspended in molar ratio 2–3 (for amounts see Table 2) in 50 ml dichloromethane under inert conditions and stirred for 0.5 h (Solution 1). CF_3SO_3H (150 mg, 0.1 mmol) was dissolved in 2.5 ml of the ionic liquid (Solution 2). Solution 1 was added to Solution 2 and stirred for 10 min. Silica (Degussa, Aerosil 355, 5 g) was ground to a powder and a sieve fraction with a particle size in the range 60–200 μm was dried overnight at 200 °C in vacuum. The silica powder was then added to the mixture and the suspension was stirred for 1 h. Finally, the suspension was frozen and the volatiles were removed, while the sample was warming slowly to give a well flowing light to dark grey powder. For comparison, a further series of samples was prepared in the same way, but without addition of $[Pd(CF_3CO_2)_2]$ and DPPF.

2.3. Physical and analytical methods

The silicon content of the supported catalysts was determined by AAS using a UNICAM 939 spectrometer. The palladium content of the catalysts was determined by neutron activation analysis (NAA). For this method, aliquots of 40 mg of each sample were enclosed in polyethylene bags and co-irradiated with a Pd-standard, and an Al–Au monitor for 5 min in position Strang-6 of the FRM-II reactor in Garching, Germany. One to seven hours after irradiation, the irradiated samples were counted successively at 10 cm distance from calibrated detectors. One day later, the samples were measured again at 2 cm distance from the detectors. The elemental content of Pd was calculated from the co-irradiated Pd standard (relative method). The internal comparator method [33] was applied to calculate the other elements in the samples. The palladium content of liquid phases was determined by AAS using a UNICAM 939 spectrometer.

Surface area and pore structure were analyzed by nitrogen adsorption at 77 K on a PMI Automated BET Sorptometer. For IR characterization, the sample was pressed into a self-supporting wafer and activated in vacuum for 1 h at 140 °C. Spectra of the sample were taken using a Bruker IFS 88 spectrometer. The spectra were recorded in the region from 4000 to 400 cm^{-1} at a resolution of 4 cm^{-1}. Scanning electron microscope images were obtained on a JEOL 500 SEM. Images were taken by operating the microscope at 23.0 kV. For transmission electron microscope images, the samples were ground, suspended in ethanol, and ultrasonically dispersed. Drops of the dispersions were applied on a copper-grid supported carbon film.

Table 2
Amounts used in the preparation of the supported catalysts

Catalyst	Silica (g)	Ionic liquid (ml)	$Pd(CF_3CO_2)_2$ (mg)	DPPF (mg)	CF_3SO_3H (mg)
$H^+/EMIm/SiO_2$	5.0	2.5	0	0	150
$Pd1/H^+/EMIm/SiO_2$	5.0	2.5	33	83	150
$Pd2/H^+/EMIm/SiO_2$	5.0	2.5	66	166	150
$Pd3/H^+/EMIm/SiO_2$	5.0	2.5	132	332	150
$H^+/BMIm/SiO_2$	5.0	2.5	0	0	150
$Pd1/H^+/BMIm/SiO_2$	5.0	2.5	33	83	150
$Pd2/H^+/BMIm/SiO_2$	5.0	2.5	66	166	150
$Pd3/H^+/BMIm/SiO_2$	5.0	2.5	132	332	150
$H^+/HMIm/SiO_2$	5.0	2.5	0	0	150
$Pd1/H^+/HMIm/SiO_2$	5.0	2.5	33	83	150
$Pd2/H^+/HMIm/SiO_2$	5.0	2.5	66	166	150
$Pd3/H^+/HMIm/SiO_2$	5.0	2.5	132	332	150
$H^+/HM_2Im/SiO_2$	5.0	2.5[a]	0	0	150
$Pd1/H^+/HM_2Im/SiO_2$	5.0	2.5[a]	33	83	150
$Pd2/H^+/HM_2Im/SiO_2$	5.0	2.5[a]	66	166	150
$Pd3/H^+/HM_2Im/SiO_2$	5.0	2.5[a]	132	332	150

[a] As HM_2Im is solid at room temperature, a molten sample was used.

Micrographs were recorded on a JEM-2010 Jeol transmission electron microscope operating at 120 kV.

For solid-state NMR, the samples were packed in 4 mm ZrO_2 rotors. ^1H MAS NMR measurements were performed on a Bruker AV600 spectrometer ($B_0 = 14.1$ T) with a spinning rate of 10 kHz. For cooling, the bearing and drive gas streams were sent through a heat exchanger in liquid nitrogen. The spectra were recorded as the sum of 16 scans using single pulse excitation with a pulse length of 2.6 μs and recycle time of 3 s. Chemical shifts are reported relative to the methylene group in adamantane ($\delta = 1.78$ ppm). ^{13}C, ^{19}F and ^{31}P MAS NMR spectra were recorded on a Bruker AV500 spectrometer ($B_0 = 11.75$ T) using a spinning rate of 15 kHz. The ^{31}P spectra were measured with proton decoupling as the sum of at least 5000 scans. Chemical shifts are reported relative to $(NH_4)H_2PO_4$ at 1.11 ppm. A recycle time of 5 s and a pulse length of 2.5 μs were used. For the ^{13}C spectra, at least 15,000 scans were recorded applying proton decoupling with 10 s recycle time and 2.5 μs pulse length. The spectra were calibrated against the methine carbon atoms of adamantane as external standard ($\delta = 29.47$ ppm). ^{19}F MAS NMR spectra were measured as single pulse experiments with a recycle rate of 2 s and a pulse length of 2.5 μs. Ten scans were recorded for each sample. The chemical shifts are reported relative to NaF ($\delta = -225$ ppm).

Reference samples for ^1H, ^{13}C, and ^{31}P NMR spectroscopy were prepared following the same procedure as for the supported catalysts except that the addition of silica was omitted. One drop of the viscous solution of the complex in the ionic liquid was dissolved in CD_2Cl_2 and transferred to an NMR tube. The samples were investigated on a Bruker AM 400 instrument using the solvent signal as internal reference.

Gas chromatography (GC) analyses were performed on a Hewlett–Packard HP 5890A gas chromatograph equipped with a cross-linked 5% diphenyl–95% dimethyl-polysiloxane column (30 m, Restek GmbH, Rtx-5 Amine) and a flame ionization detector (Temperature program: 5 min at 120 °C, 10 °C min^{-1} to 290 °C, 1 min at 290 °C). GC–MS analyses were performed on a Hewlett–Packard HP 5890 gas chromatograph equipped with an identical column and a mass selective detector HP 5971A.

2.4. Test on catalytic activity in batch mode

Experiments were performed under inert nitrogen atmosphere in a Radleys reaction carousel with 12 parallel reactors. The catalyst (0.25 g) was suspended in octane (15 ml). For two-phase catalysis, Solutions 1 and 2 (see Section 3.1) were mixed, the volatiles removed in a partial vacuum and heptane (15 ml) added. The mixture was heated to reflux at 125 °C. Aniline (1.82 ml, 20 mmol), styrene (3.44 ml, 30 mmol) and undecane (1 ml, internal GC standard) were added to each of the reactors. Samples (50 μl) were taken periodically and analyzed by GC to quantify conversion and selectivity of the reaction.

To test on leaching of palladium, reaction mixtures were prepared in same way as described above and filtered hot after either 4 or 12 h reaction time. The filtrates were kept at reflux and further samples were taken after 24 h total reaction time.

The activation energy was determined in the range 150–180 °C and 0–13% conversion using a slurry phase reactor SPR16 system (Amtec) consisting of 16 independent magnetically stirred tank reactors (pressure autoclaves). The catalyst (0.1 g) was suspended in octane (4 ml) and heated to the desired temperature. The pressure was increased to 10 bar with nitrogen. Subsequently, 4 ml of a solution of aniline (0.73 ml, 8 mmol), styrene (1.37 ml, 12 mmol) and undecane (0.4 ml) in octane were pumped into the reactor. Samples were taken automatically every 10 min and analyzed by GC.

2.5. Test on catalytic activity in fixed bed reactor

A fixed bed reactor with 115 mm length and 3 mm inner diameter was filled with catalyst (50 mg) and glass beads (remaining volume). A solution of aniline (0.10 mol l^{-1}), styrene (0.15 mol l^{-1}) and undecane (internal standard) in octane was passed over the catalyst (flow 0.2 ml min^{-1}). The temperature

was increased to 150 °C. After steady state was obtained (about 20 min), samples of the product mixture were collected at the end of the reactor for gas chromatography. Subsequently, the temperature was raised every 20 min by 10 °C to maximum 300 °C. The temperature was then reduced to 150 °C and it was confirmed that the initial activity was obtained.

2.6. Determination of the absorption constant for aniline and styrene

A fixed bed reactor was filled with catalyst (50 mg) and glass beads (remaining volume). A constant flow of octane (1 ml min^{-1}) was passed over the catalyst bed and the temperature of the reactor and feed increased to 120 °C. The concentration of aniline was then increased stepwise to 1.85×10^{-4}, 2.27×10^{-4} and 2.70×10^{-4} mol l^{-1}. The concentration of aniline at the exit was followed with UV spectroscopy at 298 nm. The uptake was calculated from the time–concentration diagram by comparison with an experiment, where the reactor had been filled only with glass beads. The experiment was repeated with styrene.

3. Results and discussion

3.1. Preparation of the supported catalysts

Bi-functional heterogeneous catalysts for the intermolecular hydroamination of styrene with aniline were obtained by immobilizing $[Pd(DPPF)](CF_3SO_3)_2$ and CF_3SO_3H in a thin film of ionic liquid on silica. Flame dried silica with a surface area of 150 $m^2 g^{-1}$ and 150–300 μm particle size was used as inert support. Note that the material had mostly mesopores and no micropores. The catalysts were prepared by wet impregnation of the silica support and were well flowing dry powders. To study systematically the effect of the ionic liquid, a series of supported catalysts $Pd/H^+/IL/SiO_2$ was prepared with imidazolium salts with decreasing polarity in the sequence EMIm, BMIm, HMIm and HM_2Im. For each catalyst $Pd/H^+/IL/SiO_2$, the palladium concentration was varied (0.011, 0.022 and 0.042 mmol g^{-1}, abbreviated $Pd1/H^+/IL/SiO_2$, $Pd2/H^+/IL/SiO_2$, $Pd3/H^+/IL/SiO_2$, respectively). The palladium content was confirmed by neutron activation analysis. As reference, a further series of catalysts $H^+/IL/SiO_2$ was prepared in the same way with CF_3SO_3H, but without palladium and phosphine ligands.

3.2. Characterization of the supported catalysts

The pore volume of the fumed silica support was determined to 0.84 $cm^3 g^{-1}$ by nitrogen adsorption. Upon adsorption of ionic liquids, a decrease of the pore volume to 0.24–0.19 $cm^3 g^{-1}$ was observed (Table 3). When the palladium complex was immobilized in the thin film of ionic liquid, the pore volume decreased linearly by 3.6(1.4) ml $mmol^{-1}_{[Pd(DPPF)](CF_3SO_3)_2}$ to 0.20–0.08 $cm^3 g^{-1}$. Closer analysis of the pore size distribution showed that pores with less than 9 nm radius were entirely filled with the ionic liquid, whereas larger pores remained unaffected (Fig. 1). In

Table 3
Elementary composition and physicochemical properties of the supported catalysts used in this study

Catalyst	Si content (calc.)[a] (wt.%)	C content (calc.)[b] (wt.%)	H content (calc.)[b] (wt.%)	N content (calc.)[b] (wt.%)	Pd content (calc.)[c] (wt.%)	Surface area[d] ($m^2 g^{-1}$)	Pore volume (ml g^{-1})
SiO_2	–	–	–	–	–	150	0.84
$H^+/EMIm/SiO_2$	23.7 (28.8)	12.70 (13.33)	1.85 (1.70)	3.98 (4.31)	–	21	0.23
$Pd1/H^+/EMIm/SiO_2$	24.0 (28.4)	13.23 (13.58)	2.01 (1.72)	4.21 (4.23)	0.11 (0.12)	16	0.15
$Pd2/H^+/EMIm/SiO_2$	22.7 (27.6)	15.73 (14.04)	2.50 (1.73)	4.04 (4.10)	0.22 (0.23)	12	0.11
$Pd3/H^+/EMIm/SiO_2$	21.0 (26.0)	14.22 (14.88)	2.20 (1.74)	3.72 (3.88)	0.40 (0.44)	11	0.11
$H^+/BMIm/SiO_2$	25.3 (29.5)	14.16 (14.85)	2.32 (2.03)	3.52 (3.74)	–	23	0.19
$Pd1/H^+/BMIm/SiO_2$	24.2 (29.1)	14.49 (15.09)	2.27 (2.03)	3.42 (3.68)	0.11 (0.12)	18	0.14
$Pd2/H^+/BMIm/SiO_2$	23.6 (28.2)	14.92 (15.52)	2.35 (2.02)	3.35 (3.57)	0.21 (0.24)	16	0.13
$Pd3/H^+/BMIm/SiO_2$	27.3 (26.6)	15.63 (16.30)	2.44 (2.02)	3.14 (3.36)	0.41 (0.45)	9	0.10
$H^+/HMIm/SiO_2$	27.2 (30.1)	15.17 (15.89)	2.26 (2.26)	3.46 (3.28)	–	24	0.24
$Pd1/H^+/HMIm/SiO_2$	25.7 (29.8)	15.77 (16.12)	2.44 (2.25)	3.11 (3.22)	0.14 (0.13)	21	0.20
$Pd2/H^+/HMIm/SiO_2$	25.0 (28.8)	17.13 (16.53)	2.63 (2.24)	2.89 (3.12)	0.23 (0.24)	17	0.17
$Pd3/H^+/HMIm/SiO_2$	25.7 (27.2)	16.39 (17.26)	2.51 (2.22)	3.12 (2.94)	0.43 (0.46)	10	0.08
$H^+/HM_2Im/SiO_2$	26.4 (30.2)	15.38 (16.58)	2.53 (2.40)	2.82 (3.13)	–	28	0.23
$Pd1/H^+/HM_2Im/SiO_2$	25.5 (29.8)	15.76 (16.79)	2.37 (2.38)	2.61 (3.08)	0.12 (0.13)	23	0.19
$Pd2/H^+/HM_2Im/SiO_2$	26.0 (28.9)	16.52 (17.17)	2.51 (2.36)	2.85 (2.99)	0.24 (0.24)	19	0.15
$Pd3/H^+/HM_2Im/SiO_2$	24.1 (27.2)	16.75 (17.87)	2.62 (2.34)	2.47 (2.82)	0.41 (0.46)	14	0.10

As additional information, neutron activation analysis provided the trace content of lanthanum and manganese, which was as follows (in mg kg^{-1}): 11.9, 10.3 ($Pd1/H^+/EMIM/SiO_2$); 5.3, 3.28 ($Pd2/H^+/EMIM/SiO_2$); 0.572, 1.16 ($Pd3/H^+/EMIM/SiO_2$); 5.66, 3.00 ($Pd1/H^+/BMIM/SiO_2$); 5.54, 2.99 ($Pd2/H^+/BMIM/SiO_2$); 8.97, 1.68 ($Pd3/H^+/BMIM/SiO_2$); 1.23, 1.19 ($Pd1/H^+/HMIM/SiO_2$); 2.52, 1.3 ($Pd2/H^+/HMIM/SiO_2$); 9.33, 1.52 ($Pd3/H^+/HMIM/SiO_2$); 5.64, 3.57 ($Pd1/H^+/HM_2IM/SiO_2$); 5.82, 4.25 ($Pd2/H^+/HM_2IM/SiO_2$); 5.95, 4.00 ($Pd3/H^+/HM_2IM/SiO_2$), respectively. Other trace metals were not detected. (Calc.) Values in brackets correspond to the calculated value.

[a] Silicon content determined by atomic absorption spectroscopy.

[b] CHN analysis.

[c] Palladium content determined by neutron activation.

[d] BET surface area determined by N_2 adsorption at 77 K.

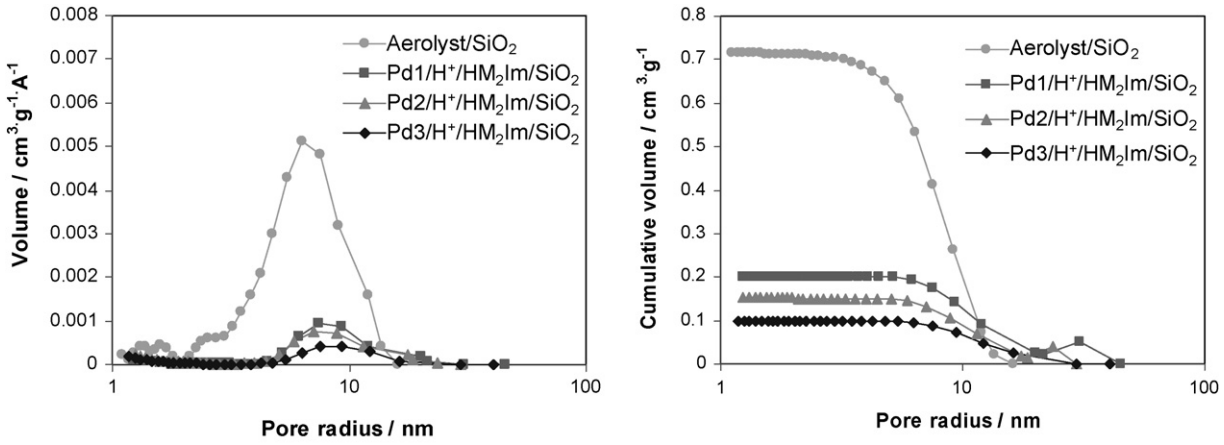

Fig. 1. Analysis of the pore size distribution (left) and cumulative pore size distribution (right) for the catalyst series $Pd/H^+/HM_2Im/SiO_2$ in comparison to the parent silica.

consequence, the surface area decreased considerably upon impregnation with ionic liquid (from 150 to 28–21 $m^2\,g^{-1}$) and after immobilization of the palladium complex (23–9 $m^2\,g^{-1}$).

Electron micrographs of the support showed silica particles of 150–300 μm diameter, which consisted of spherical primary particles of approximately 10 nm radius. After coating, the particles were observed in scanning electron microscopy with much higher precision (Fig. 2). This effect can be attributed to the electric conductivity of the thin film of ionic liquid. Based on the concentration of supported ionic liquid a theoretical film thickness of 3 nm was calculated. However, the film was not observed directly in the transmission electron micrographs (resolution *ca.* 1 nm). Therefore, we conclude that the majority of the ionic liquid molecules were not part of an even, physisorbed film on the silica surface, but rather filled preferentially smaller mesopores leading to thinner coatings on the outer surface or in larger pores.

IR spectroscopy (Fig. 3) was used to characterize the surface chemistry. With the parent support, a band at 3745 cm^{-1} characteristic of silanol groups was observed. The broad band at 3594 cm^{-1} is assigned to internal hydrogen bonded hydroxyl groups. Upon adsorption of the ionic liquid, the band corresponding to terminal SiOH groups disappeared, while a new broad band appeared at 3320 cm^{-1}. This indicates that all silanol groups interact with the ionic liquid *via* hydrogen bonds. Thus, we conclude that the entire silica surface is covered by the ionic liquid, but it is not possible to deduce the actual thickness of the layer. The IR spectra of the supported catalysts showed several bands corresponding to the ionic liquids at 2700–3300 cm^{-1} (asymmetric and symmetric stretching vibrations of CH_3 and CH_2 groups), 1700–1600 cm^{-1} (C=C stretching vibration) and 1500–1300 cm^{-1} (CH bending vibrations).

The ^1H MAS NMR spectrum of EMIm dissolved in CD_2Cl_2 is shown in Fig. 4(a). The signals due to the 1-ethyl-3-methylimidazolium cation are readily distinguished. They are assigned to the alkyl-methyl group (1.54 ppm), the N-bound methyl group (3.94 ppm), the N-bound methylene group (4.27 ppm), and the protons in the 4, 5, and 2 position of the imidazolium ring (7.47, 7.53, and 8.70 ppm), respectively. When EMIm was supported on silica, the widths of all lines increased significantly (Fig. 4(b)). This increase was much more pronounced, when $[Pd(DPPF)(CF_3CO_2)_2]$ and CF_3SO_3H were immobilized in the supported ionic liquid (Fig. 4(c)). Note that the chemical shift of the resonances remained unchanged, when $[Pd(DPPF)(CF_3CO_2)_2]$ was immobilized (within ±0.1 ppm).

In the ^{13}C MAS NMR spectra of the supported catalysts (Fig. 5), the line-widths of the carbon nuclei in the imidazolium-based cation were between 25 and 63 Hz (Table 4). The values compare to line-widths of 2–3 Hz for the neat ionic liquids. A slight high-field shift of the CH_2–N signal is observed with increasing length of the ionic liquid in the order EMIm < BMIm < HMIm < HM_2Im. In the spectrum of $Pd3/H^+/HM_2Im/SiO_2$, the additional methyl group gave rise to a resonance at 13.96 ppm. In addition, the N=C–N signal was shifted to higher field. Small signals were observed at 75, 78, 130 and 134 ppm. They are assigned to the cyclopentadienyl ring in the ferrocene part (75 and 78 ppm) and the phosphorus bound phenyl rings (130 and 134 ppm) of the 1,1′-bis(diphenylphosphino)ferrocene ligand.

The immobilized complexes were probed by ^{19}F and ^{31}P MAS NMR. The ^{19}F MAS NMR spectra of the catalysts were very similar showing a resonance at −78.7 ppm with a pronounced shoulder on the low-field side (not shown). In agreement with previous studies the main resonance is assigned to trifluoromethane sulphonate anions [34], whereas the shoulder corresponds to trifluoroacetate anions [35]. Differences between free and coordinating mono-dentate anions were not observed, in agreement with previous studies [35]. Therefore, it is not possible to determine, which anions bind to the Pd^{2+} cation in the complex.

In the ^{31}P MAS NMR spectra of the immobilized catalysts, the line broadening was similar to that in the ^1H and ^{13}C MAS NMR spectra. In all spectra, a single resonance was observed at 47.3 ppm and assigned to the phosphine ligand of the palladium complex. The line-width was between 440 and 1360 Hz. In comparison, the $^{31}P\{^1H\}$ NMR signal for a solution of $[Pd(DPPF)(CF_3CO_2)_2]$, CF_3SO_3H and IL in CD_2Cl_2,

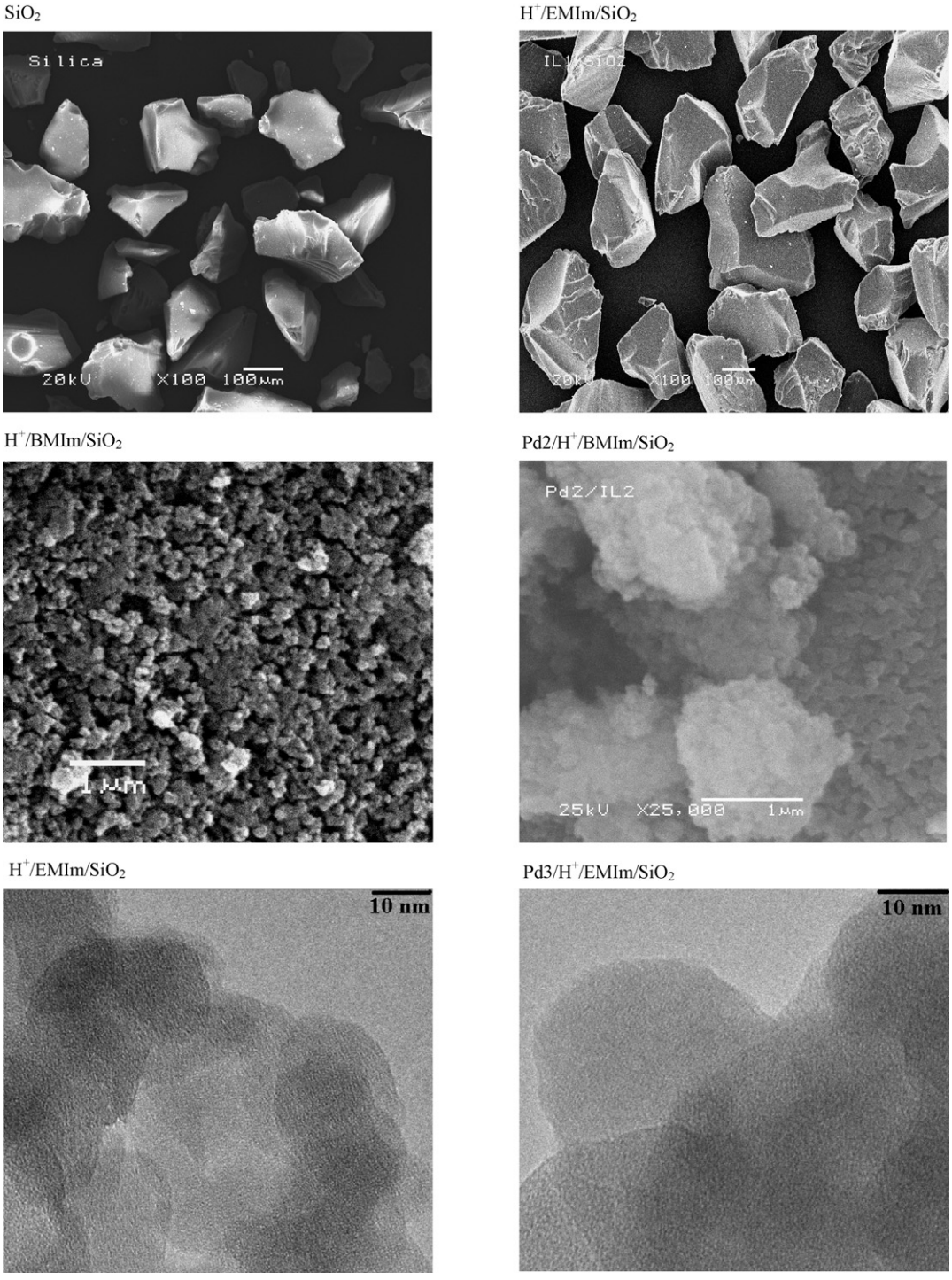

Fig. 2. Scanning electron micrographs (upper two rows) and transmission electron micrographs (bottom) of selected catalysts.

was observed at 47.1 ppm with a line-width of only 2.5 Hz (IL = EMIm, BMIm, HM_2Im).

In general, NMR spectra of solids have broader peaks than the liquid state NMR spectra of the same substance. The reason for this is related to the chemical shift anisotropy and the fact that the hetero-nuclear dipolar coupling is not averaged out by rotation of the molecules. The latter effect can be minimized by magic angle spinning (MAS) [36]. In the present case, the spectra were independent of the rotation speed, when it exceeded 5000 Hz. Thus, coupling constants to other nuclei in the sample were well below 5000 Hz. Decreasing tumbling rates of the probed molecule also lead to a decrease of T2, where T2 is the time constant for transverse relaxation—the loss of magnetization in the *x*–*y* plane [37]. Decrease in T2 also leads to broadening of the resonances in the NMR spectrum. The changes in line-width observed for spectra of immobilized catalysts, in particular, for those containing palladium complexes, are assigned to differences in the T2 relaxation time, which is not influenced by MAS.

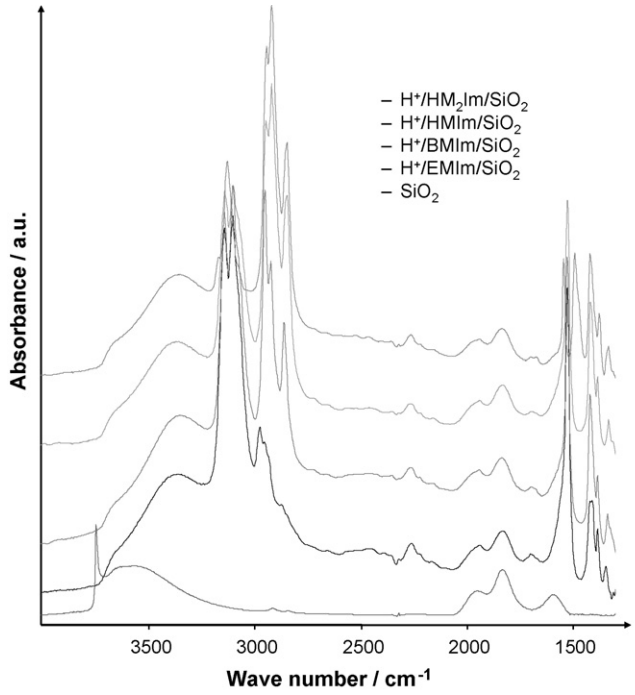

Fig. 3. Infrared spectra of the supported ionic liquids in comparison with the parent silica.

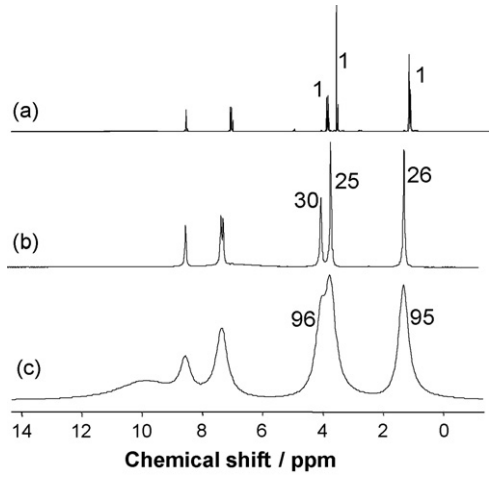

Fig. 4. (a) Liquid state ^{1}H NMR spectrum of EMIm; (b) solid-state ^{1}H NMR spectrum of H^+/EMIm/SiO_2; (c) solid-state ^{1}H NMR spectrum of Pd3/H^+/EMIm/SiO_2. Numbers are referring to line-width in Hz.

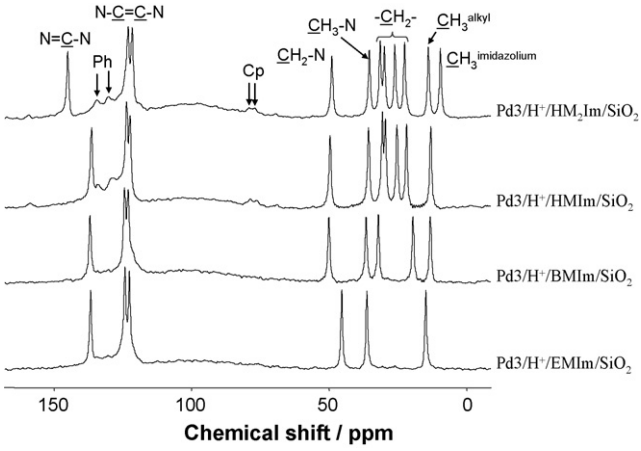

Fig. 5. ^{13}C MAS NMR spectra of the supported catalysts.

Vice versa, NMR line-widths can be taken as a measure for the mobility of a particular atomic group [31,38–40]. As the Fe^{2+} ion in the ferrocene part of the ligand has only paired electrons, the spectra are not affected by paramagnetic interactions (leading also to line broadening). The same is true for Pd^{2+} due to its square planar coordination.

This interpretation is supported by dissolution of [Pd(DPPF)$(CF_3CO_2)_2$] and CF_3SO_3H in the unsupported ionic liquids. A large increase in viscosity compared to the parent ionic liquid [41] was observed confirming that the mobility of the molecules was considerably lowered. The increase in the line-width of the ^{31}P resonance showed that interaction with the ionic liquids reduced the mobility of the palladium complex significantly compared to the same complex in CD_2Cl_2.

Marked differences were observed, when the ^{1}H MAS NMR spectra of different supported ionic liquids were compared (Table 5). The line-width of the nitrogen bound methyl and methylene groups increased with increasing size of the imidazolium cation in the order H^+/EMIm/SiO_2 <

Table 4
Position and line-width of the signals due to the imidazolium cations in ^{13}C NMR spectroscopy

Catalyst	N–*C*=*C*–N		N=*C*–N		N–*C*H_2		N–*C*H_3		Alkyl–*C*H_3	
	Position (ppm)	Line-width (Hz)	Position (ppm)	Line-width (Hz)	Position (ppm)	Line-width (Hz)	Position (ppm)	Line-width (Hz)	Position (ppm)	Line-width (Hz)
Pd3/H^+/EMIm/SiO_2	122.53 124.21	30.14 30.54	136.63	30.62	45.45	26.25	36.33	27.44	14.95	25.67
Pd3/H^+/BMIm/SiO_2	123.06 124.31	61.64 60.06	136.86	53.88	50.08	51.39	36.57	63.56	13.23	52.39
Pd3/H^+/HMIm/SiO_2	122.34 123.56	48.47 57.80	136.34	57.65	49.64	55.06	35.66	53.27	13.13	51.97
Pd3/H^+/HM_2Im/SiO_2	121.52 123.02	39.56 32.99	144.86	32.99	49.01	35.77	35.41	33.22	9.58	32.33

Table 5
Position and line-width of the signals due to imidazolium cations in ^{1}H NMR spectroscopy

Catalyst	N=C(*H*)–N		N–C*H*$_2$		N–C*H*$_3$		Alkyl–C*H*$_3$	
	Position (ppm)	Line-width (Hz)	Position (ppm)	Line-width (Hz)	Position (ppm)	Line-width (Hz)	Position (ppm)	Line-width (Hz)
H^+/EMIm/SiO_2	8.59	26	4.10	30	3.77	25	1.35	26
H^+/BMIm/SiO_2	8.64	25	4.07	32	3.80	27	0.75	25
H^+/HMIm/SiO_2	8.70	33	4.08	41	3.81	32	0.71	27
H^+/HM_2Im/SiO_2	–	–	4.01	49	3.70	48	0.75	28
Pd3/H^+/EMIm/SiO_2	8.54	122	4.08	98	3.76	96	1.34	95
Pd3/H^+/BMIm/SiO_2	8.65	516	4.08	333	3.79	332	0.79	307
Pd3/H^+/HMIm/SiO_2	8.64	307	4.07	263	3.77	384	0.70	147
Pd3/H^+/HM_2Im/SiO_2	–	–	4.03	286	3.70	424	0.81	169

H^+/BMIm/SiO_2 < H^+/HMIm/SiO_2 < H^+/HM_2Im/SiO_2 (Fig. 6) indicating that the mobility of the aromatic ring decreased with increasing size of the imidazolium cation. In contrast to this, the line-width of the terminal methyl group in the alkyl side chain was equal (25–28 Hz) for all ionic liquids showing that the methyl groups in the alkyl chain maintained a certain degree of rotational freedom independent of the size of the cation.

Similar trends were observed for the series of immobilized catalysts Pd3/H^+/IL/SiO_2. The line-width of the nitrogen bound methyl and methylene group in the ^{1}H MAS NMR spectra was significantly higher than of the terminal methyl group of the alkyl chain (Fig. 6). However, a maximum in the line-width of the N–CH_2 and the alkyl–CH_3 groups was observed for Pd3/H^+/BMIm/SiO_2. In particular, the line-width of the methyl group in the hexyl chain was much lower than that in the butyl chain. It is concluded that the first four carbon atoms of the alkyl chains contribute most to the intermolecular interactions between the IL and the palladium complexes, whereas the ends of longer alkyl chains maintain some structural flexibility. It has been shown that hydrophobic interactions between alkyl chain and the aromatic rings of the phosphine ligand lead to domain formation [31,42]. The line-widths in NMR spectra provide, therefore, a sensitive probe for the intensity of such interactions.

For each resonance in the ^{1}H NMR spectra of the immobilized catalysts, a single Lorentzian shaped peak was observed. This shows that all IL cations are chemically equivalent within the NMR time scale suggesting that the ionic liquid did not coordinate directly to the palladium center in [Pd(DPPF)(CF_3CO_2)$_2$]. All ionic liquid molecules in the supported ionic liquid were on average equally affected by the presence of the palladium complex. Note that the catalysts contained Pd^{2+}, DPPF, CF_3SO_3H and ionic liquid in a molar ratio of 1:1.5:2.5:25–33. An alternative explanation would be rapid exchange of coordinated and free imidazolium cations resulting in a split of the peaks, when the temperature is decreased. However, this was not observed in NMR measurements at variable temperature between 223 and 373 K (*vide infra*) (Fig. 7).

The present data are in agreement with the formation of ordered domains caused by the immobilization of a palladium complex in the ionic liquids [31]. We suggest that the imidazolium cations form a solvent cage around the palladium complexes (Fig. 8), thereby establishing a long-range ordered system [43,44], which in turn is responsible for the reduced mobility. Similar domain formation has been suggested for metal nano-particles in imidazolium ionic liquids [45,46].

The formation of these solvent cages involves disruption of inter-ionic Coulomb interactions between the ionic liquid anions and cations [31], which results in the perturbation of the local structure of the ionic liquid [47]. In an attempt to minimize the potential energy, the spheres of ionic liquid molecules around the complexes assume a minimum size. The observation of a single set of signals in the NMR spectra and considering the molar ratio of complex to ionic liquid show that the solvent cage around one complex molecule consists of up to 25–33 ion pairs of the ionic liquid. The aggregates arrange to a regular packing with glass-like structure.

The dynamic interaction of the ionic liquid and Pd complex was investigated by temperature resolved MAS NMR experi-

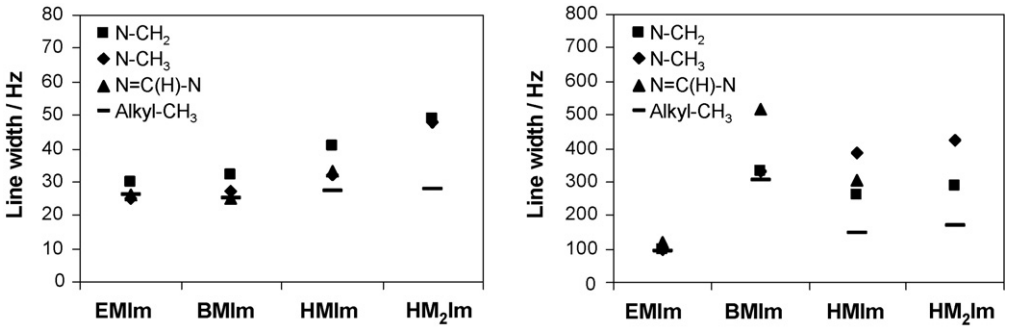

Fig. 6. Line-width observed for the catalysts H^+/IL/SiO_2 (left) and Pd3/H^+/IL/SiO_2 (right).

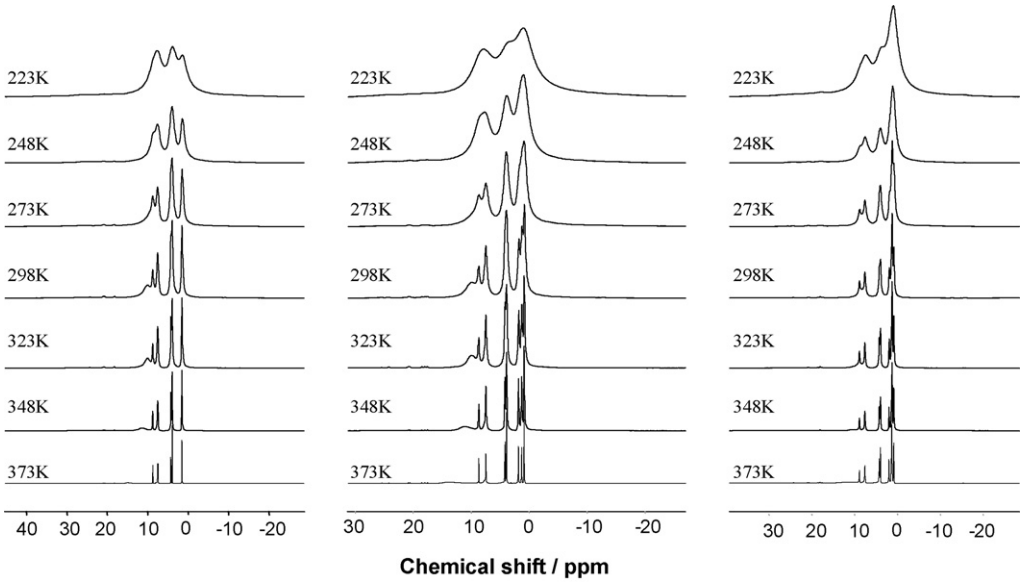

Fig. 7. Temperature dependent ^{1}H MAS NMR spectra of the supported catalysts: Pd3/H$^+$/EMIm/SiO$_2$ (left), Pd3/H$^+$/BMIm/SiO$_2$ (middle), Pd3/H$^+$/HMIm/SiO$_2$ (right).

ments. For all samples, the line-width of all peaks decreased exponentially with temperature. A change of slope in the logarithmic plot (Fig. 9) shows that a phase transition from glassy to liquid state occurred at *ca.* 348 K (Pd3/H$^+$/EMIm/SiO$_2$ and Pd3/H$^+$/BMIm/SiO$_2$). For Pd3/H$^+$/HMIm/SiO$_2$, the phase transition occurred above 373 K. After the phase transition, the line-width in the spectra of the Pd3/H$^+$/IL/SiO$_2$ samples was similar to that of the H$^+$/IL/SiO$_2$ series at 298 K. This indicates that the solvent cages break down and the molecules acquire similar mobility to the parent supported liquid, which does not contain the dissolved complex.

Closer inspection of the ^{1}H MAS NMR spectra of the catalysts (Fig. 10) revealed a broad signal around 10 ppm (at 298 K), which was assigned to the acidic proton of CF_3SO_3H. The peak was shifted downfield and broadened, when the temperature was increased to 348 K. These changes were irreversible. A low-field shift corresponds to deshielding of the probed nucleus, in other words a decrease of the electron density at the proton. This observation indicates that the Brønsted acidity of the sample increased, when the catalyst was activated at temperatures of 348 K or above. It is speculated that trace amounts of water were removed, which participated in exchange reactions with the acidic proton while present.

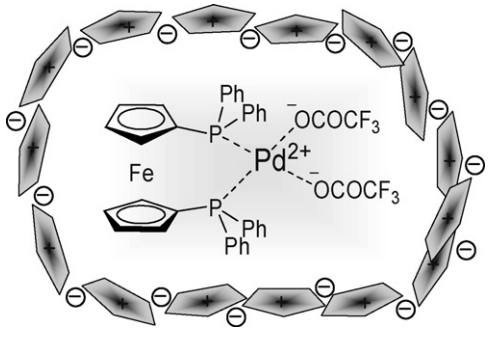

Fig. 8. Artist's impression of the solvent cage of ionic liquid molecules around the organometallic palladium complex.

3.3. Catalytic activity of the supported catalysts

The catalytic activity and selectivity was explored in the addition of aniline to styrene (Eq. (3)):

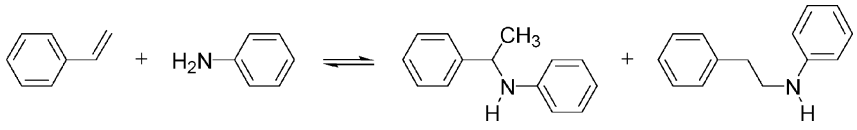

(3)

At 125 °C in a batch reactor the Markownikoff product *N*-(1-phenyl-ethyl)-aniline was formed with a selectivity of 100% over all catalysts (based on aniline conversion). The selectivity based on styrene was lower (50–95%), as oligomerization occurred as side reaction. The activity of the catalysts increased in the sequence $HM_2Im < HMIm < BMIm < EMIm$ (Fig. 11). Thus, the IL with higher polarity provided a higher activity. The initial catalytic activity was linearly correlated with the Pd loading, which corresponds to first order in palladium. However, catalytic activity was only observed, when the palladium concentration exceeded $\sim 9 \times 10^{-3}$ $mmol_{Pd^{2+}}$ g_{Cat}^{-1}. We suggest that for all catalysts an equal amount of the palladium complex was strongly adsorbed to the silica surface and did not participate in the catalytic reaction.

The stability of the supported catalysts was investigated in filtration tests, in which the solid catalyst was removed from the reaction mixture after 4 or 12 h, respectively. The result-

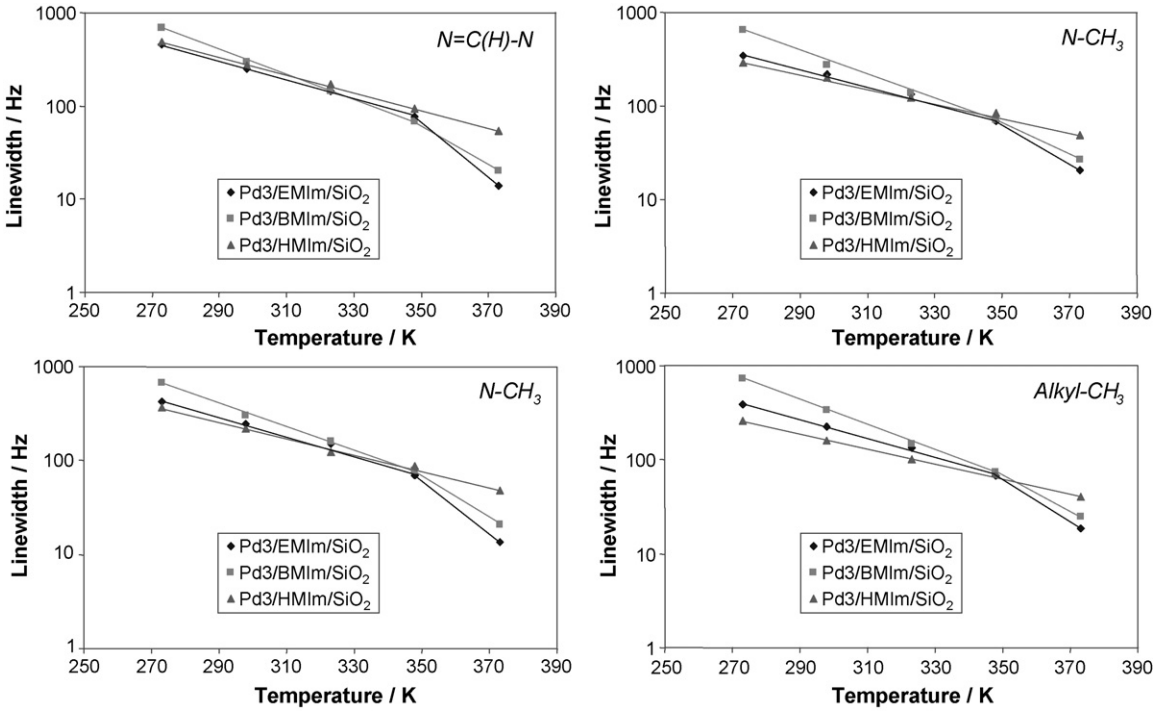

Fig. 9. Line-width in ^{1}H NMR spectroscopy as a function of temperature for selected protons.

ing filtrates did not exhibit catalytic activity. We conclude that leaching of the palladium catalyst into the bulk organic phase does not occur. Moreover, the palladium content in the catalysts remained constant and palladium was not found in the filtrate (detection limit 10^{-6} mol l^{-1}).

The initial turnover frequency was 33.3 mol $(\text{mol}_{\text{Pd}^{2+}}\ \text{h})^{-1}$ for the catalyst Pd3/H^{+}/EMIm/SiO$_2$ with 0.042 mmol$_{\text{Pd}^{2+}}$ g_{Cat}^{-1}. In comparison, for the homogeneous catalyst a turnover frequency of 7 h^{-1} was reported, albeit in a different solvent (toluene) [12]. The same bi-functional catalyst was tested in two-phase catalysis (EMIm–heptane) and almost the same turnover frequency was observed (32.2 mol $(\text{mol}_{\text{Pd}^{2+}}\ \text{h})^{-1}$). When the catalytically inactive palladium in Pd3/H^{+}/EMIm/SiO$_2$ is considered, the turnover frequency per metal center was slightly higher for the supported catalyst (42.4 mol $(\text{mol}_{\text{Pd}^{2+}}\ \text{h})^{-1}$). Approximately equal activity strongly suggests the absence of diffusion limitations across the liquid–liquid phase-boundary, as the area of the liquid–liquid interface is much higher for the supported catalyst in comparison with the two-phase catalysis. The palladium complex is virtually insoluble in heptane and the reaction must, therefore, take place in the bulk of the ionic liquid phase. This is in agreement with good solubility of aniline in the ionic liquid. In this respect, the absorption constant for aniline into the supported ionic liquid phase was determined to 0.204, 0.221, and 0.235 mmol g^{-1} for HM$_2$Im, BMIm, and EMIm, respectively [32]. Considering that part of the adsorbed aniline was either protonated, or bound to Pd (aniline/Pd = 2/1), the physically dissolved aniline concentration calculates to 0.001, 0.018, and 0.037 mmol g^{-1}, respectively. Styrene has a low solubility in the ionic liquids used in this

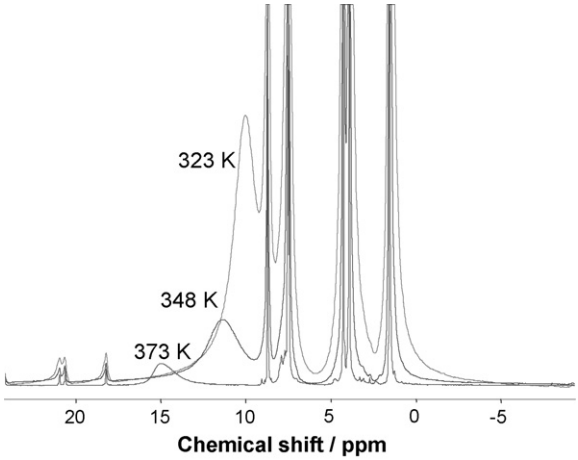

Fig. 10. Irreversible shift of the acidic protons to lower field upon heating.

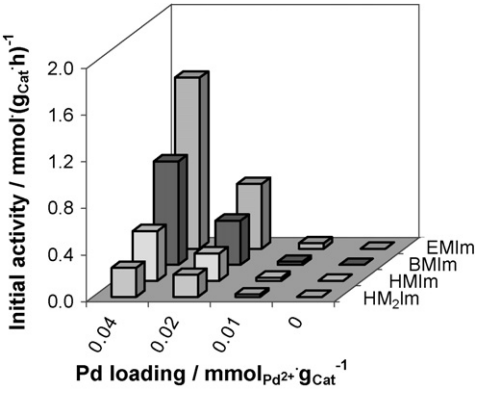

Fig. 11. Catalytic activity of the supported catalysts in the addition of aniline to styrene.

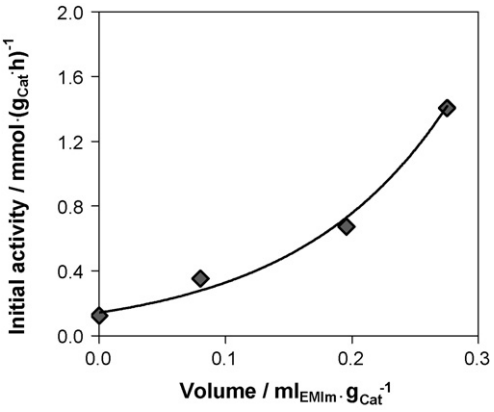

Fig. 12. Dependence between the amount of ionic liquid and the catalytic activity of supported catalysts.

study. However, co-absorption of aniline and styrene leads to enhanced styrene uptake [14].

The amount of supported ionic liquid strongly influenced the catalytic activity. In a series of catalysts varying in the amount of the ionic liquid, but with the same palladium content, the catalytic activity increased with increasing amount of the ionic liquid (Fig. 12). These results suggest either that a minimum of at least 33 ion pairs (*vide supra*) of the ionic liquid were required to solvate the palladium complex entirely or that the turnover frequency per metal atom increased. Note that in this series the molar ratio of ion pairs of the ionic liquid to palladium was 0, 8, 16, and 33.

The reaction was studied in further detail at reaction temperatures up to 300 °C using a fixed bed reactor. Conversion of aniline started at 150 °C (Fig. 13). With increasing temperature, the activity of the catalysts increased exponentially to reach a maximum at approximately 240 °C. Steady-state conversion of 65% at this temperature (EMIm based catalyst, 0.044 $mmol_{Pd^{2+}}\ g_{Cat}^{-1}$) corresponds to an integral reaction rate of 8.4 $mmol\,(g_{Cat}\,h)^{-1}$ and a turnover frequency of 199 $mol\,(mol_{Pd^{2+}}\,h)^{-1}$. The Markownikoff isomer *N*-(1-phenyl-ethyl)-aniline was formed exclusively at lower

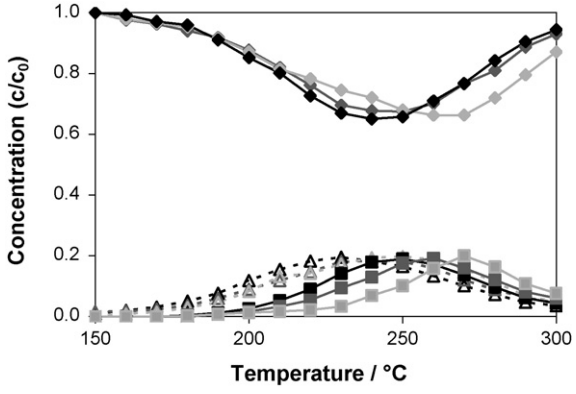

Fig. 13. Temperature–concentration profile for the addition of aniline to styrene catalyzed by Pd3/H^+/IL/SiO_2 in the fixed bed reactor (IL = EMIm, BMIm, HM_2Im; black, dark grey and light grey symbols, respectively). The concentration of aniline (diamonds), *N*-(1-phenyl-ethyl)-aniline (open triangles) and *N*-(2-phenyl-ethyl)-aniline (squares) at the exit of the fixed bed reactor are shown.

temperatures, whereas at higher temperatures the corresponding *anti*-Markownikoff isomer *N*-(2-phenyl-ethyl)-aniline was also observed. At temperatures above 250 °C, the conversion decreased as the thermodynamic limit of the (slightly exothermic) reaction was encountered. In the thermodynamic regime, the ratio of the Markownikoff to the *anti*-Markownikoff product was similar for all catalysts (0.77(3), 0.75(1) and 0.65(4) for the EMIm, BMIm and HM_2Im based catalyst, respectively) and nearly independent of the temperature.

The activity of the three catalyst series for formation of *N*-(1-phenyl-ethyl)-aniline was similar in the kinetic regime, decreasing slightly in the sequence EMIm > BMIm > HM_2Im (Fig. 13). At 200 °C, e.g., the relative concentration of the Markownikoff product at the reactor exit was 1.43:1.08:1, respectively. This is consistent with the activation energy measured in batch experiments in the temperature range 150–180 °C. For the catalysts based on EMIm, BMIm, HMIm, and HM_2Im (0.042 $mmol_{Pd^{2+}}\ g_{Cat}^{-1}$), the activation energy was 88, 74, 55 and 46 kJ mol^{-1} (based on aniline consumption). Within the error of measurement (±5 kJ mol^{-1}), the activation energy calculated from the formation of the Markownikoff product was equal (81, 69, 54 and 46 kJ mol^{-1}, respectively). Note that in the batch experiments, the formation of small amounts of the *anti*-Markownikoff product *N*-(2-phenyl-ethyl)-aniline was observed at 180 °C. Similarly, formation of *N*-(2-phenyl-ethyl)-aniline was observed in the fixed-bed reactor at temperatures above 180 °C. For the *anti*-Markownikoff product, the differences in catalyst activity were much higher compared to the Markownikoff product. At 220 °C (230 °C), e.g., the relative concentration of the *anti*-Markownikoff product at the reactor exit for the EMIm, BMIm, and HM_2Im based catalyst was 4.3:2.6:1 (4.3:2.9:1).

Several mechanisms for hydroamination have been discussed in literature [3,12,16,32,48]. Two mechanisms appear most likely for Lewis acidic late transition metal complexes in the presence of a Brønsted acid (Fig. 14): nucleophilic attack on a coordinated styrene (path A) and insertion of styrene into a palladium–hydride bond as key step (path B). We conclude that the formation of the Markownikoff product follows the mechanistic path A. Coordination of styrene to the palladium *via* the olefin π-bond renders it susceptible to a nucleophilic attack of the lone electron pair at the aniline nitrogen atom. Formal 1,3-proton shift from the ammonio-group to the α-carbon atom and protolytic cleavage of the metal–carbon bond is rate determining.

The catalytic tests in the batch mode were performed at the upper limit of the thermal stability of the solvent cages. We speculate that the considerably higher rate of reaction in the ionic liquid phase compared to classic solvents [see also 15,32] is related to acceleration of the rate-determining step. Most likely, the ammonio proton is transferred more readily to the α-carbon atom, as it remains caught within the solvent cage. The anions of the ionic liquid might play a key role in this respect and function as proton shuttle, whereby the most polar ionic liquid (EMIm) is most effective. The acidic conditions in the ionic liquid phase also help in preventing loss of the proton from vicinity of the reactive center. Possibly, metal–substrate interactions are also

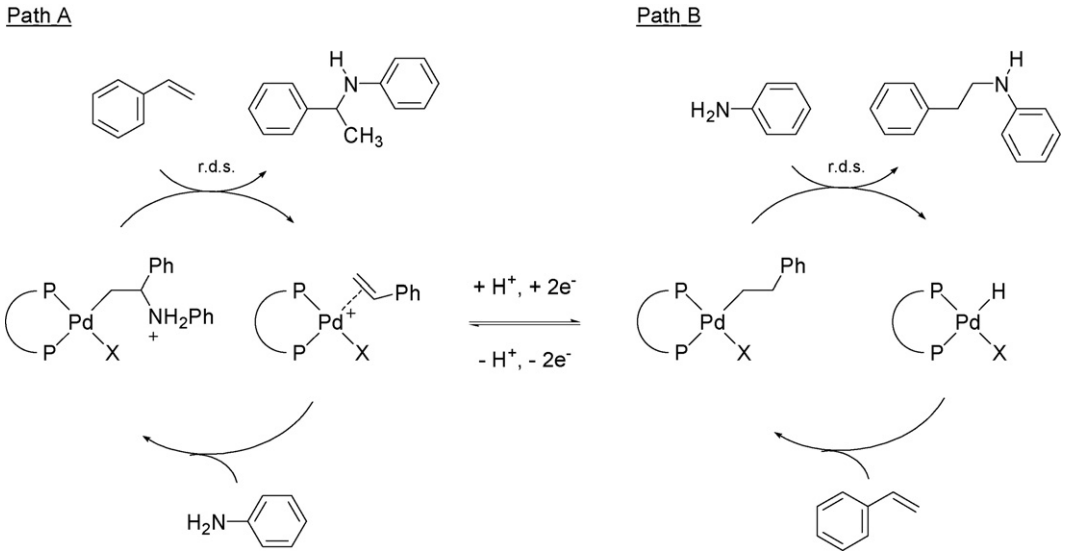

Fig. 14. Reaction mechanism proposed for formation of *N*-(1-phenyl-ethyl)-aniline and *N*-(2-phenyl-ethyl)-aniline (X = $CF_3SO_3^-$).

enhanced within the solvent cage. At 200 °C, the solvent cages are no longer stable and the ionic liquid functions as classic solvent. Small differences in activity within the series of ionic liquids are speculated to be caused by differences in polarity. Improved stabilization of a polar transition state associated with the rate-determining step [49] in the more polar environment leads to higher intrinsic rate of reaction. Note that this is in agreement with the relatively high activation energy observed for the most active catalyst (Pd3/H^+/EMIm/SiO_2), which is indicative of a higher frequency factor.

For formation of the *anti*-Markownikoff product, we suggest mechanistic path B. A palladium hydride is formed in an initial reduction step. The olefinic double bond of styrene is subsequently inserted into the Pd–H bond. Nucleophilic attack (r.d.s.) of the lone electron pair of the aniline nitrogen atom at the α-carbon atom provides the *anti*-Markownikoff product, which desorbs from the coordination sphere of the palladium.

In case of mechanistic path B, the product distribution is determined by the regioselectivity of the insertion step. The steric demand of the phenyl group allows only formation of the 2-phenyl-ethyl palladium complex, whereas during formation of the 1-phenyl-ethyl palladium complex strong steric conflicts would arise between the phenyl-group of styrene and the phenyl groups at the phosphine. Formation of the *anti*-Markownikoff product was, therefore, observed only at high temperatures, at which the solvent cages were no longer stable. The higher aniline concentration in the ionic liquid phase with higher polarity is speculated to lead to higher turnover frequencies in the rate-determining step.

The kinetic data indicate that a reversible reaction links the two mechanistic pathways. We speculate that the palladium complex with coordinated styrene (path B) reacts with a hydride source to the 2-phenylethyl palladium complex (path A). The hydride source might be styrene reacting to phenylacetylene.

4. Conclusions

The concept of immobilizing palladium complexes in a thin film of supported ionic liquid has been proven functional for assembling novel bi-functional hydroamination catalysts. The concept combines advantages of homogeneous catalysis (optimum utilization of metal centers, tunable selectivity) with those of heterogeneous catalysis (facile recovery of catalyst, application in continuous processes). We have shown the practicability of the concept for the addition of aniline to styrene, where Lewis acidic palladium complexes are excellent catalysts. The reaction rate was higher compared to classic solvents and increased with increasing palladium loading and increasing polarity of the ionic liquid. Detailed characterization of the supported catalysts showed that solvent cages of ionic liquid are formed around the palladium complexes. The ordering effect leads to a drastically reduced mobility of ionic liquid and complex molecules. Within the solvent cage, the rate-determining step – 1,3-proton shift and protolytic cleavage of the palladium–carbon bond in the 2-ammonio ethyl complex – is accelerated. Differences in the catalytic activity depending on the choice of ionic liquid are accounted to different ability of the ionic liquids to act as proton shuttle. At higher temperatures, the solvent cages break down and the ionic liquid functions as classic solvent. Here, the differences in activity are less pronounced. Interestingly, formation of the *anti*-Markownikoff product *N*-(2-phenyl-ethyl)-aniline was also observed at temperatures above 180 °C.

The present report gives evidence for the influence of ordered three-dimensional structures onto the catalytic performance of palladium complexes supported in a thin film of ionic liquid. The ordering effect can be utilized to induce unusual properties in the organometallic complexes. Possible applications include the enhancement of metal–substrate interactions, the reorientation of substrate molecules within in the solvent cage during a two-step catalytic process, and the possibility of directing the approach of molecules to catalytically active centers.

Conflict of interest

As the study has been funded by public sources, there are no potential conflicts of interests.

Acknowledgements

Max-Buchner Forschungstiftung is thanked for a providing a grant to OJ. The authors are grateful to Andreas Spirkl, Xaver Hecht and Martin Neukamm for support during the experimental work.

References

[1] T.E. Müller, in: I.T. Horváth (Ed.), Encyclopedia of Catalysis, Wiley, New York, 2002, p. 492.
[2] R. Taube, in: B. Cornils, W.A. Herrmann (Eds.), Applied Homogeneous Catalysis with Organometallic Compounds, vol. 1, VCH, Weinheim, 1996.
[3] T.E. Müller, M. Beller, Chem. Rev. 98 (1998) 675.
[4] I. Bytschkov, S. Doye, Eur. J. Org. Chem. (2001) 4411.
[5] E. Haak, I. Bytschkov, S. Doye, Angew. Chem. Int. Ed. 38 (1999) 3389.
[6] M. Nobis, B. Drießen-Hölscher, Angew. Chem. Int. Ed. 40 (2001) 3983.
[7] C.G. Hartung, A. Tillack, H. Trauthwein, M. Beller, J. Org. Chem. 66 (2001) 6339.
[8] T. Shimada, Y. Yamamoto, J. Am. Chem. Soc. 124 (2002) 12670.
[9] M. Tokunaga, M. Ota, M. Haga, Y. Wakatsuki, Tetrahedron Lett. 42 (2001) 3865.
[10] M. Beller, H. Trauthwein, M. Eichberger, C. Breindl, J. Herwig, T.E. Müller, O.R. Thiel, Chem. Eur. J. 5 (1999) 1306.
[11] M. Beller, O.R. Thiel, H. Trauthwein, C. Hartung, Chem. Eur. J. 6 (2000) 2513.
[12] M. Kawatsura, J.F. Hartwig, J. Am. Chem. Soc. 122 (2000) 9546.
[13] J. Penzien, R.Q. Su, T.E. Müller, J. Mol. Catal. 182 (2002) 489.
[14] J. Bodis, T.E. Müller, J.A. Lercher, Green Chem. 5 (2003) 227.
[15] V. Neff, T.E. Müller, J.A. Lercher, J. Chem. Soc., Chem. Commun. 8 (2002) 906.
[16] H.M. Senn, P.E. Blöchl, A. Togni, J. Am. Chem. Soc. 122 (2000) 4098.
[17] K. Tanabe, W.F. Hölderich, Appl. Catal. A 181 (1999) 399.
[18] A. Chauvel, B. Delmon, W.H. Hölderich, Appl. Catal. 115 (1994) 173.
[19] O. Jiménez, T.E. Müller, W. Schwieger, J.A. Lercher, J. Catal. 239 (2006) 42.
[20] M. Tada, M. Shimamoto, T. Sasaki, Y. Iwasawa, Chem. Commun. (2004) 2562.
[21] J. Penzien, C. Haeßner, A. Jentys, K. Köhler, T.E. Müller, J.A. Lercher, J. Catal. 221 (2004) 302.
[22] J. Penzien, A. Abraham, J.A. van Bokhoven, A. Jentys, T.E. Müller, C. Sievers, J.A. Lercher, J. Phys. Chem. 108/13 (2004) 4116.
[23] S. Breitenlechner, M. Fleck, T.E. Müller, A. Suppan, Mol. Catal. A: Chem. 214 (2004) 175.
[24] A. Corma, H. Garcia, Chem. Rev. 103 (2003) 4307.
[25] M.H. Valkenberg, C. de Castro, W.F. Hölderich, Green Chem. 4 (2002) 88.
[26] E. Benazzi, H. Olivier, Y. Chauvin, J.F. Joly, A. Hirschauer, Abstr. Pap. Am. Chem. Soc. 212 (1996) 45.
[27] J. Huang, T. Jiang, H. Gao, B. Han, Z. Liu, W. Wu, Y. Chang, G. Zhao, Angew. Chem. 116 (2004) 1421.
[28] M.H. Valkenberg, C. de Castro, W.F. Hölderich, Appl. Catal. A: Gen. 215 (2001) 185.
[29] M.H. Valkenberg, C. de Castro, W.F. Hölderich, Top. Catal. 14 (2001) 139.
[30] C.P. Mehnert, R.A. Cook, N.C. Dispenziere, M. Afeworki, J. Am. Chem. Soc. 124 (2002) 12932.
[31] C. Sievers, O. Jiménez, T.E. Müller, S. Steuernagel, J.A. Lercher, J. Am. Chem. Soc. 128 (2006) 13990.
[32] O. Jiménez, T.E. Müller, C. Sievers, A. Spirkl, J.A. Lercher, Chem. Commun. (2006) 2974.
[33] X. Lin, R. Henkelmann, Anal. Bioanal. Chem. 379 (2004) 210.
[34] D. Sirbu, G. Consiglio, B. Milani, P.G.A. Kumar, P.S. Pregosin, S. Gischig, J. Organomet. Chem. 690 (2005) 2254.
[35] K.J. Snowden, T.R. Webb, B. Snoddy, Inorg. Chem. 32 (1993) 3541.
[36] D.D. Laws, H.-M.L. Bitter, A. Jerschow, Angew. Chem. Int. Ed. 41 (2002), 3096 and references cited therein.
[37] T.D.W. Claridge, High-Resolution NMR Techniques in Organic Chemistry, Elsevier, Oxford, 1999.
[38] A. Lauenstein, J. Tegenfeldt, J. Phys. Chem. B 101 (1997) 3311.
[39] A. Johansson, J. Tegenfeldt, J. Chem. Phys. 104 (1996) 5317.
[40] R. Spindler, D.F. Shriver, J. Am. Chem. Soc. 110 (1988) 3036.
[41] P. Bonhote, A.P. Dias, N. Papageorgiou, K. Kalyanasundaram, M. Gratzel, Inorg. Chem. 35 (1996) 1168.
[42] Y. Wang, G.A. Voth, J. Am. Chem. Soc. 127 (2005) 12192.
[43] R. Atkin, G.G. Warr, J. Am. Chem. Soc. 127 (2005) 11940.
[44] R.A. Mantz, P.C. Trulove, R.T. Carlin, R.A. Osteryoung, Inorg. Chem. 34 (1995) 3846.
[45] P. Migowski, J. Dupont, Chem. Eur. J. 13 (2007) 32.
[46] C.W. Scheeren, G. Machado, S.R. Teixeira, J. Morais, J.B. Domingos, J. Dupont, J. Phys. Chem. B 110 (2006) 13011.
[47] L. Crowhurst, N.L. Lancaster, J.M.P. Arlandis, T. Welton, J. Am. Chem. Soc. 126 (2004) 11549.
[48] U. Nettekoven, J.F. Hartwig, J. Am. Chem. Soc. 124 (2002) 1166.
[49] T.E. Müller, M. Berger, M. Grosche, E. Herdtweck, F.P. Schmidtchen, Organometallics 20 (2001) 4384.